ARTICLE IN PRESS

Nuclear Inst. and Methods in Physics Research, A xxx (xxxx) xxx

Contents lists available at ScienceDirect

Nuclear Inst. and Methods in Physics Research, A

journal homepage: www.elsevier.com/locate/nima

Calibration of the Belle II aerogel ring imaging detector

R. Pestotnik [i,*], I. Adachi [a,b], L. Burmistrov [c], F. Le Diberder [c], R. Dolenec [d], K. Hataya [e], S. Kakmimoto [e], H. Kakuno [e], H. Kawai [f], T. Kawasaki [g], H. Kindo [b], T. Konno [g], S. Korpar [h,i], P. Križan [d,i], T. Kumita [e], Y. Lai [a], M. Machida [j], M. Mrvar [i], S. Nishida [a,b], K. Noguchi [e], K. Ogawa [k], S. Ogawa [l], L. Šantelj [a], T. Sumiyoshi [e], M. Tabata [f], S. Tamechika [e], M. Yonenaga [e], M. Yoshizawa [k], Y. Yusa [k]

[a] High Energy Accelerator Research Organization (KEK), Tsukuba, Japan
[b] SOKENDAI (The Graduate University of Advanced Science), Tsukuba, Japan
[c] Laboratoire de Laccelerateur Lineaire (LAL), Orsay, France
[d] University of Ljubljana, Slovenia
[e] Tokyo Metropolitan University, Hachioji, Japan
[f] Chiba University, Japan
[g] Kitasato University, Sagamihara, Japan
[h] University of Maribor, Slovenia
[i] Jožef Stefan Institute, Ljubljana, Slovenia
[j] Tokyo University of Science, Noda, Japan
[k] Niigata University, Niigata, Japan
[l] Toho University, Funabashi, Japan

ARTICLE INFO

Keywords:
Proximity focusing RICH with an aerogel radiator
Particle identification algorithm
Extended maximum likelihood

ABSTRACT

For efficient separation of hadrons in the forward end-cap of the Belle II spectrometer, an aerogel proximity focusing Ring Imaging Detector is installed in the high magnetic field between the central drift chamber and electromagnetic calorimeter. Cherenkov photons, emitted in the double layer aerogel radiator are expanded through the empty space and detected on the photon detector consisting of Hybrid Avalanche Photo diodes. The readout electronics working in a threshold mode records hit patterns registered during beam collisions. A particle identification algorithm based on the two dimensional extended maximum likelihood technique is used to assign probabilities for different particle hypotheses of tracks traversing the aerogel RICH detector. For efficient discrimination, the Aerogel RICH detector has to be calibrated. We present the key calibration steps used to optimize the detector performance.

1. Introduction

Belle II Aerogel Ring Imaging Cherenkov Counter (ARICH) aims to identify hadrons with high efficiency over wide interesting momentum range from 0.5 to 4 GeV/c [1]. It has to primarily separate kaons from pions. In addition it should be able to separate muons from pions in the low momentum range from about 0.5 GeV/c to 1 GeV/c. The detector consists of two 2 cm thick layers of aerogel radiator in a focusing configuration ($n_1 = 1.045$ and $n_2 = 1.055$), a 16 cm thick expansion volume and a photon detector plane equipped with 420 Hybrid Avalanche Photo diodes with front-end boards mounted at the back (Fig. 1) [2–4]. The detector covers about 3.5 m^2 in the forward end-cap region of the Belle II spectrometer and is located in the 1.5 T magnetic field perpendicular to the photon detector plane. In order not to loose photons, planar mirrors are positioned at the outer edge of a donut-like detector. The data from up to six front-end boards are serialized in one merger board and send via an optical fiber to the common acquisition system outside of the spectrometer.

The Aerogel RICH was installed in the Belle II spectrometer in the summer 2017. In the following months, the detector has been gradually connected to the power supplies and to the common readout. After initial tests, the detector has been included in the common Belle II spectrometer acquisition, where cosmic ray events were recorded. At the end of April 2018, the Belle II spectrometer started to take data originating from collision events.

The detector has been partially operational [5]. There were several HAPDs exhibiting too high currents and were switched off. Parts of the detector was not working due to a malfunctioning of the trigger signal. Due to temperatures which reached 70 °C in the hottest areas of the

* Corresponding author.
E-mail address: Rok.Pestotnik@ijs.si (R. Pestotnik).

https://doi.org/10.1016/j.nima.2019.01.027
Received 31 October 2018; Received in revised form 7 January 2019; Accepted 10 January 2019
Available online xxxx
0168-9002/

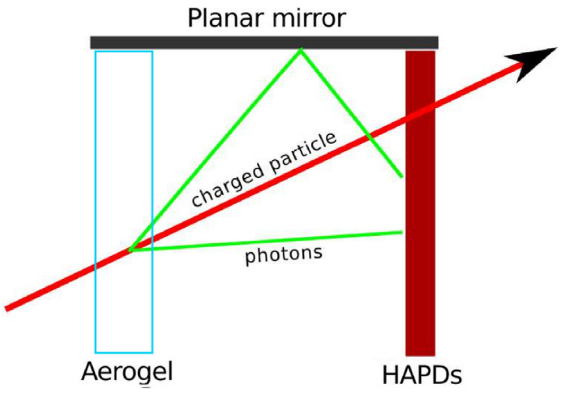

Fig. 1. Principle of the Aerogel RICH: A cone of Cherenkov photons emitted in the aerogel is projected on the photon detector (HAPDs). Photons at the edges are reflected by planar mirrors towards the photon detector.

detector and which might affect the operation of the HAPD photo sensor, about one half of the detector was not powered during the beam collision data taking. Those problems were identified and resolved during the 2018 autumn shutdown. Trigger cables have been replaced and the cooling system of the Aerogel RICH upgraded, so that the temperatures are expected not to exceed 40 degrees, well in the sensor operating specifications.

2. Identification algorithm

The particle identification in ARICH is based on the evaluation of maximum likelihood function for different particle hypotheses h for each track. The construction of the likelihood function follows P. Baillon [6] and R. Forty [7]. The likelihood function consists of a product of probabilities p_i of individual pixels i being hit

$$L = \prod_{\text{all pixels}} p_i \quad \text{where} \quad p_i = \frac{e^{-n_i} {n_i}^{m_i}}{m_i!}, \tag{1}$$

The probability of pixel i recording m_i hits is Poissonian, where n_i is the expected i.e. calculated average number of hits on the particular pixel. Since binary hit information is used, the probabilities for a pad to be hit ($m_i > 0$) or not ($m_i = 0$) can be simplified

$$p_i = \begin{cases} e^{-n_i} & \text{for } m_i = 0, \\ 1 - e^{-n_i} & \text{for } m_i > 0. \end{cases} \tag{2}$$

After separating contributions from hit and non-hit pixels and constraining the number of expected hits N for a given hypothesis to the sum of expected average number of hits on the detector we obtain

$$lnL = -N + \sum_{\text{hit } i} n_i + ln(1 - e^{-n_i}) \, . \tag{3}$$

The advantage of this procedure is that one now has to calculate the average number of hits, i.e. the hit probabilities n_i only for the hit pixels.

One is thus left with the calculation of expected average numbers of hits on the pixels which have detected at least one photo electron. This number is a sum of contributions of signal hits and background hits, $n_i = n_s^i + n_b^i$. The signal n_s^i includes contributions from different radiator layers r: $n_s^i = \sum n_{s,r}^i$. The contribution of each radiator to the signal on the individual pixel is calculated according to:

$$n_{s,r}^i = \varepsilon_i n_{t,r} \int_{\Omega_i} S_r(\theta_r, \phi_r) d\theta_r d\phi_r, \tag{4}$$

where we assumed a detection efficiency ε_i to be constant over the surface of pixel i. By $n_{t,r}$ we denote the total number of photons emitted in a specific radiator r for a given hypothesis. The integral runs over the solid angle Ω_i subtended by the individual pixel and

$$S_r(\theta_r, \phi_r) = \frac{1}{2\pi} \frac{1}{\sqrt{2\pi}\sigma_{\theta_r}} e^{-\frac{(\theta_r - \theta_r^h)^2}{2\sigma_{\theta_r}^2}} \tag{5}$$

is the probability for a Cherenkov photon being emitted by particle h, from radiator r into the solid angle $d\theta_r d\phi_r$ at θ_r and ϕ_r relative to the track direction and σ_{θ_r} is the Cherenkov angle resolution.

The likelihood is evaluated for different particles in the sample. A discrimination cut is set based on a requirement for purity of the sample. Identification efficiency is then defined as a ratio between a number of particles surviving the cut and a number of all particles.

3. Detector performance

The detector performance depends on the understanding of its function and response. Therefore in parallel with the detector design and installation a particle identification algorithm has been tested first on the simulation.

The detector response has been simulated in the Belle II analysis and simulation framework BASF2 [8] based on Geant4 libraries [9]. The simulation of the Aerogel RICH detector includes a high energy particle tracking in the Aerogel RICH, a generation of Cherenkov photons in the aerogel radiator and in the quartz window of the photo sensor, tracking of the photons through the aerogel, the expansion volume and the photo sensor. Optical tracking includes possible reflections from planar mirrors installed in the barrel part of the detector and ends with the photon detection in the photo-cathode of the photo sensor. The detected hits are converted to digits to mimic the binary response of the electronics. This ensures that the data format of the simulated events is the same as the measured data format.

To determine particle identification capabilities of the Aerogel RICH, particles will be used, which can be identified by other Belle II spectrometer subsystems independently from the Aerogel RICH. An example of such particles are $D^{\pm *}$ mesons, which can decay through different channels resulting in D meson and either a pion or a photon as the decay products. In the case of the $D^{\pm *} \to D^0 + \pi^{\pm}$ decays, the pion is relatively slow and its charge determines the identity of the particle from the D^0 meson decay. Identification efficiency can be determined by fitting the D^0 invariant mass before and after applying a cut on the Aerogel RICH likelihood value.

From the simulation results we expect that the kaon identification efficiency will be above 90% at a rather low pion misidentification rate of about 5% over wide momentum range from 0.5 GeV/c to 4 GeV/c (Fig. 2).

Unfortunately, the number of kaons (72) and pions (84) from $D^{\pm *}$ decays, collected during the first months of the Belle II operation was too low to evaluate the efficiency.

4. Calibration

Calibration of the detector is necessary due to its direct impact on the algorithm performance. In the likelihood function the calibration reflects in the number of expected photons per pixel n_i with contributions from background and signal. The signal part depends on the detection efficiency of the pad ε_i (Eq. (4)) and the probability density function (Eq. (5)) through the Cherenkov angle resolution σ_{θ_r}. A non-calibrated detector thus decreases the identification efficiencies and increases the misidentification probabilities.

The calibration of the detector is performed in several steps. First the operational parameters of the detector components have been measured. The detector was then calibrated using the acquired data. As a last step and an important input to further physics analyses is the determination of the efficiencies and misidentification probabilities on the beam collision data.

Please cite this article as: R. Pestotnik, I. Adachi, L. Burmistrov et al., Calibration of the Belle II aerogel ring imaging detector, Nuclear Inst. and Methods in Physics Research, A (2019), https://doi.org/10.1016/j.nima.2019.01.027.

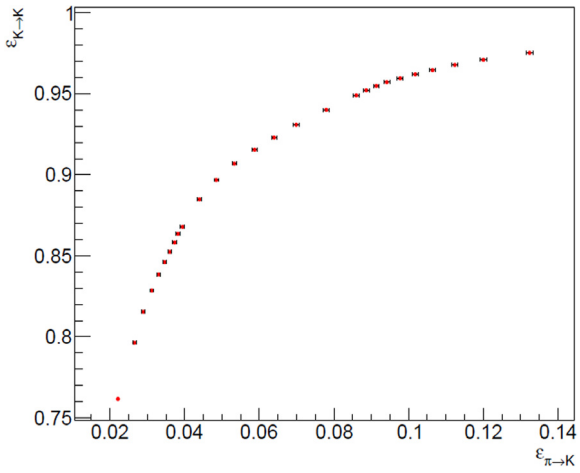

Fig. 2. Simulated kaon identification efficiency as a function of a pion misidentification probability for particles from $D^{\pm *}$ decays.

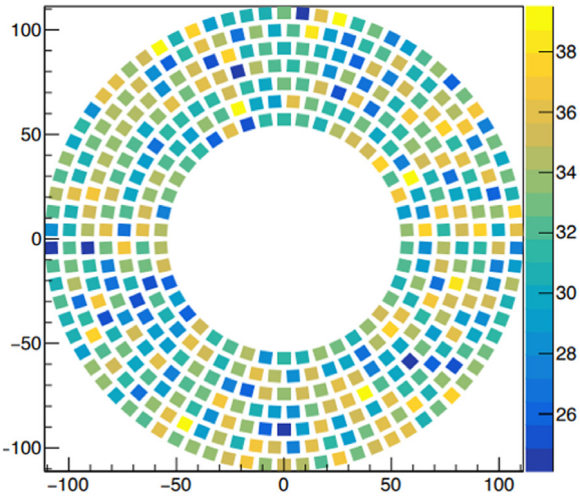

Fig. 3. Distribution of quantum efficiency of the installed sensors.

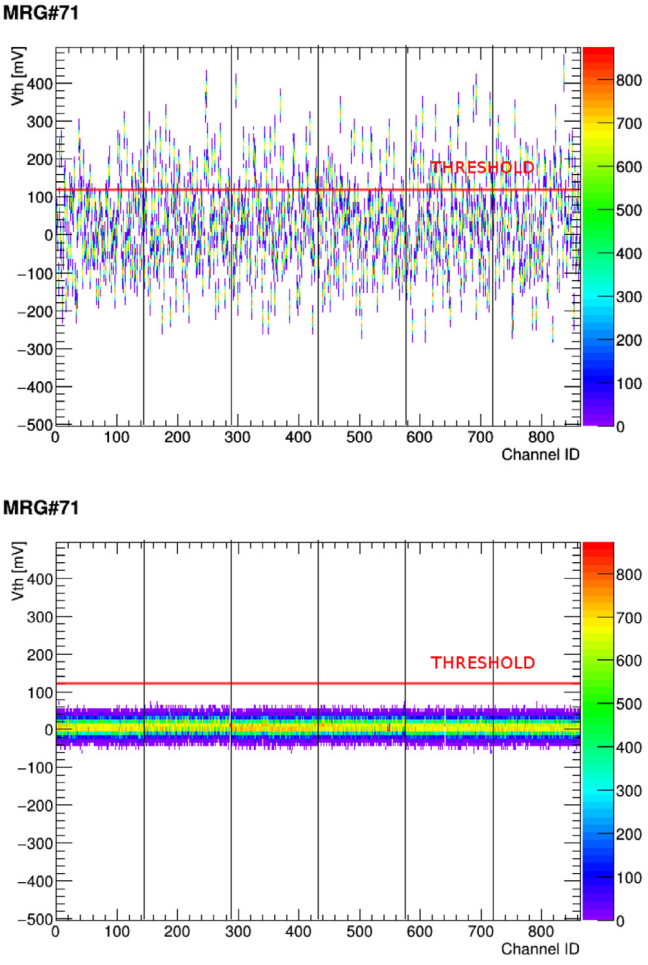

Fig. 5. Response of the detector for different channels and threshold voltages for one merger board with six front-end boards connected. Upper plot: non-calibrated offsets, lower plot: calibrated offsets. The measurement is triggered randomly, so that only the baseline with noise is sample.

Before the installation the photo sensor operation parameters have been determined (e.g. High and APD Bias voltages). A refractive index and a transmission length of the aerogel tiles have been measured and monitored throughout the production. The variations of the measured values are small and the aerogel tiles were randomly distributed in the mounting frame during the installation. We measured a position dependence of the quantum efficiency. In Fig. 3, the efficiency averaged over the surface is shown. Note that the spread is not negligible, since only minimal value of quantum efficiency was one of the production specifications. To equalize the detector performance, the mounting positions of HAPDs were selected randomly as well.

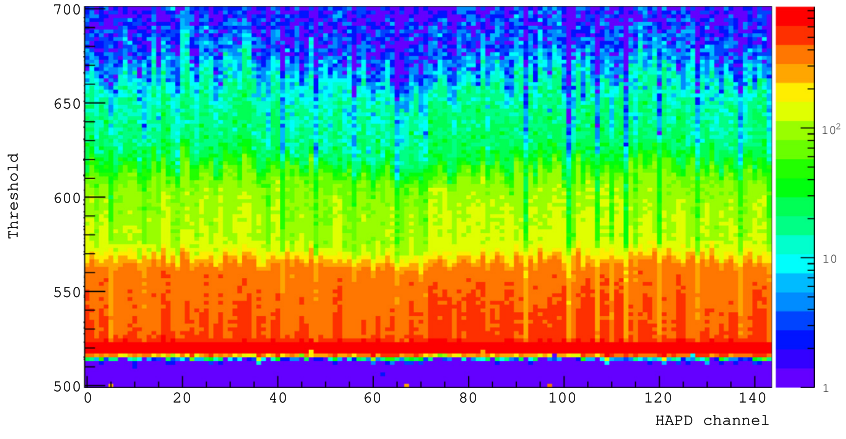

Fig. 4. Laser scan over the centers of sensor channels. The response of an illuminated channel to different threshold voltages is shown.

Please cite this article as: R. Pestotnik, I. Adachi, L. Burmistrov et al., Calibration of the Belle II aerogel ring imaging detector, Nuclear Inst. and Methods in Physics Research, A (2019), https://doi.org/10.1016/j.nima.2019.01.027.

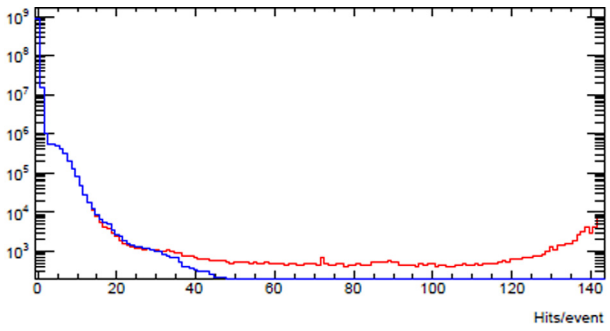

Fig. 6. Distribution of the number of hits per sensor per event. All sensor hits (red) and accepted hits (blue). (For interpretation of the references to color in this figure legend, the reader is referred to the web version of this article.)

We scanned the surface of the sensor over the centers of the channels, and measured its response to short low intensity laser pulses at different discriminator values (Fig. 4). From the plot the gain of the channels can be extracted. We expect the gain will slowly decrease during the operation due to irradiation, which will have to be compensated by adjustment of the front end board ASIC gain and shaping time.

All the measured and calculated parameters were stored in a central experiment database, from where the reconstruction algorithms can access them.

During the Aerogel RICH operation, different parameters are constantly monitored to ensure a reliable operation. We are logging the high and bias voltages and currents of the HAPD sensor, temperatures and supply voltages of the front-end and merger boards.

Before the data acquisition, the front-end boards need to be programmed to set the ASIC common gain and discrimination threshold and channel dependent offsets. An example of a calibration of the channel offsets is shown in Fig. 5. From the upper plot offsets are calculated and uploaded to the detector. One common threshold can then be used to discriminate between hit and non-hit channels.

In the laboratory tests, the response to the laser beam focused on the channel centers was used. In the Aerogel RICH detector, the LED light (λ = 470 nm) emitted from the LEDs and distributed through optical fibers to 90 points between the photo sensors is used. The light, reflected from the aerogel surface, will be regularly used to determine the noisy and dead channels, relative sensitivity and gain of each channel.

During the beam collision data acquisition the quality of the data is monitored constantly. In the event based filter, the HAPD sensors with too many hits are rejected (see Fig. 6). Monitoring of dead and noisy channels is done for each run and new channels that appear are used for further reconstruction. Cherenkov angle distribution for saturated rings is used to calculate the number of detected photons per event. With the procedure described above the detection efficiency of each hit ε_i and the total number of photons per hypothesis N can be then be calculated.

To complete the calibration the Cherenkov angle resolution σ_{θ_r} has to be optimized by alignment of the detector [10]. From displacements on different positions of the detector, new alignment constants are determined, leading to correct σ_{θ_r}, which can then be used in the algorithm.

5. Summary

Proximity focusing RICH with aerogel as the radiator is installed in the Belle II spectrometer for efficient particle identification in the forward end-cap of the Belle II spectrometer.

The detector requires a calibration in order to determine the Cherenkov angle resolution, background and the number of detected Cherenkov photons, quantities that directly impact the identification algorithms.

After the calibration we expect to meet the expectations from beam tests and simulation studies. Based on the experiences with running the detector we will establish the calibration procedures to ensure optimal operation of the detector in the future.

Acknowledgments

We thank the SuperKEKB group for excellent operation of the accelerator; the KEK cryogenics group for efficient solenoid operations; and the KEK computer group. The authors acknowledge the financial support from MEXT Japan and the Slovenian Research Agency, Slovenia (research core funding No. P1-0135).

References

[1] T. Abe, et al., Belle II Technical design report, arXiv:1011.0352 [physics.ins-det].
[2] M. Tabata, et al., Springer Proc. Phys. 212 (2018) 253–256.
[3] S. Nishida, et al., Nucl. Instrum. Methods A 595 (2008) 150.
[4] R. Pestotnik, et al., Front end electronics of the Belle II Aerogel Ring Imaging detector, this proceedings.
[5] H. Kindo, et al., this proceedings, NIMA_PROCEEDINGS-D-18-00584.
[6] P. Baillon, Nucl. Instrum. Methods A 238 (1985) 341.
[7] R. Forty, Nucl. Instrum. Methods A 433 (1999) 257–261.
[8] T. Kuhr, et al., arXiv:1809.04299v1 [physics.comp-ph].
[9] S. Agostinelli, et al., Nucl. Instrum. Methods A 506 (2003) 250–303;
J. Allison, et al., IEEE Trans. Nucl. Sci. 53 (1) (2006) 270–278;
J. Allison, et al., Nucl. Instrum. Methods A 835 (2016) 186–225.
[10] S. Tamechika, et al., this proceedings, NIMA_PROCEEDINGS-D-18-00594.

Please cite this article as: R. Pestotnik, I. Adachi, L. Burmistrov et al., Calibration of the Belle II aerogel ring imaging detector, Nuclear Inst. and Methods in Physics Research, A (2019), https://doi.org/10.1016/j.nima.2019.01.027.